Diagnostic Accuracy of Multiparametric MRI versus Ga-PSMA-11 PET/MRI for Extracapsular Extension and Seminal Vesicle Invasion in Patients with Prostate Cancer

Muehlematter, Urs J ; Burger, Irene A ; Becker, Anton S ; Schawkat, Khoschy ; Hötker, Andreas M ; Reiner, Cäcilia S ; Müller, Julian ; Rupp, Niels J ; Rüschoff, Jan H ; Eberli, Daniel ; Donati, Olivio F

Abstract: Background Recent studies have reported the additive value of combined gallium 68 (Ga)-labeled Glu-urea-Lys (Ahx)-HBED-CC ligand targeting the prostate-specific membrane antigen (PSMA) (hereafter called Ga-PSMA-11) PET/MRI for the detection and localization of primary prostate cancer compared with multiparametric MRI. Purpose To compare the diagnostic accuracy and interrater agreement of multiparametric MRI and Ga-PSMA-11 PET/MRI for the detection of extracapsular extension (ECE) and seminal vesicle infiltration (SVI) in patients with prostate cancer. Materials and Methods Retrospective analysis of 40 consecutive men who underwent multiparametric MRI and Ga-PSMA-11 PET/MRI within 6 months for suspected prostate cancer followed by radical prostatectomy between April 2016 and July 2018. Four readers blinded to clinical and histopathologic findings rated the probability of ECE and SVI at multiparametric MRI and PET/MRI by using a five-point Likert-type scale. The prostatectomy specimen served as the reference standard. Accuracy was assessed with a multireader multicase analysis and by calculating reader-average areas under the receiver operating characteristics curve (AUCs), sensitivity, and specificity for ordinal and dichotomized data in a region-specific and patient-specific approach. Interrater agreement was assessed with the Fleiss multirater . Results For multiparametric MRI versus PET/MRI in ECE detection, respectively, AUC, sensitivity, and specificity in the region-specific analysis were 0.67 and 0.75 (.07), 28% (21 of 76) and 47% (36 of 76) (.09), and 94% (529 of 564) and 90% (509 of 564) (.007). For the patient-specific analysis, AUC, sensitivity, and specificity were 0.66 and 0.73 (.19), 46% (22 of 48) and 69% (33 of 48) (.04), and 75% (84 of 112) and 67% (75 of 112) (.19), respectively. For multiparametric MRI versus PET/MRI in SVI detection, respectively, AUC, sensitivity, and specificity of the region-specific analysis were 0.66 and 0.74 (.21), 35% (seven of 20) and 50% (10 of 20) (.25), and 98% (295 of 300) and 94% (282 of 300) (< .001). For the patient-specific analysis, AUC, sensitivity, and specificity were 0.65 and 0.79 (.25), 35% (seven of 20) and 55% (11 of 20) (.20), and 98% (137 of 140) and 94% (131 of 140) (.07), respectively. Interrater reliability for multiparametric MRI versus PET/MRI did not differ for ECE (, 0.46 vs 0.40; = .24) and SVI (, 0.23 vs 0.33; = .39). Conclusion Our results suggest that gallium 68 (Ga)-labeled Glu-urea-Lys (Ahx)-HBED-CC ligand targeting the prostate-specific membrane antigen (PSMA) (Ga-PSMA-11) PET/MRI and multiparametric MRI perform similarly for local staging of prostate cancer in patients with intermediate-to-high-risk prostate cancer. The increased sensitivity of Ga-PSMA-11 PET/MRI for the detection of extracapsular disease comes at the cost of a slightly reduced specificity. © RSNA, 2019.

DOI: https://doi.org/10.1148/radiol.2019190687

Journal Article
Published Version

Originally published at:
Muehlematter, Urs J; Burger, Irene A; Becker, Anton S; Schawkat, Khoschy; Hötker, Andreas M; Reiner, Cäcilia S; Müller, Julian; Rupp, Niels J; Rüschoff, Jan H; Eberli, Daniel; Donati, Olivio F (2019). Diagnostic Accuracy of Multiparametric MRI versus Ga-PSMA-11 PET/MRI for Extracapsular Extension and Seminal Vesicle Invasion in Patients with Prostate Cancer. Radiology, 293(2):350-358.
DOI: https://doi.org/10.1148/radiol.2019190687

Radiology

ORIGINAL RESEARCH • GENITOURINARY IMAGING

Diagnostic Accuracy of Multiparametric MRI versus ^{68}Ga-PSMA-11 PET/MRI for Extracapsular Extension and Seminal Vesicle Invasion in Patients with Prostate Cancer

*Urs J. Muehlematter, MD** • *Irene A. Burger, MD** • *Anton S. Becker, MD, PhD* • *Khoschy Schawkat, MD* • *Andreas M. Hötker, MD* • *Cäcilia S. Reiner, MD* • *Julian Müller, MD* • *Niels J. Rupp, MD* • *Jan H. Rüschoff, MD* • *Daniel Eberli, MD* • *Olivio F. Donati, MD*

From the Institute of Diagnostic and Interventional Radiology (U.J.M., A.S.B., K.S., A.M.H., C.S.R., O.F.D.), Department of Nuclear Medicine (U.J.M., I.A.B., J.M.), Department of Pathology and Molecular Pathology (N.J.R., J.H.R.), and Department of Urology (D.E.), University Hospital Zurich, University of Zurich, Rämistrasse 100, Zurich 8091, Switzerland; and Department of Nuclear Medicine, Kantonsspital Baden, Baden, Switzerland (I.A.B.). Received March 26, 2019; revision requested May 16; final revision received July 24; accepted August 5. **Address correspondence to** U.J.M. (e-mail: *urs.muehlematter@usz.ch*).

I.A.B. supported by GE Medical Systems through an institutional research grant for PSMA PET/MRI studies. K.S. supported (for living expenses only) by the Swiss National Science Foundation and the Swiss Society of Radiology.

*U.J.M. and I.A.B. contributed equally to this work.

Conflicts of interest are listed at the end of this article.

Radiology 2019; 00:1–9 • https://doi.org/10.1148/radiol.2019190687 • Content codes: GU MR

Background: Recent studies have reported the additive value of combined gallium 68 (^{68}Ga)-labeled Glu-urea-Lys (Ahx)-HBED-CC ligand targeting the prostate-specific membrane antigen (PSMA) (hereafter called ^{68}Ga-PSMA-11) PET/MRI for the detection and localization of primary prostate cancer compared with multiparametric MRI.

Purpose: To compare the diagnostic accuracy and interrater agreement of multiparametric MRI and ^{68}Ga-PSMA-11 PET/MRI for the detection of extracapsular extension (ECE) and seminal vesicle infiltration (SVI) in patients with prostate cancer.

Materials and Methods: Retrospective analysis of 40 consecutive men who underwent multiparametric MRI and ^{68}Ga-PSMA-11 PET/MRI within 6 months for suspected prostate cancer followed by radical prostatectomy between April 2016 and July 2018. Four readers blinded to clinical and histopathologic findings rated the probability of ECE and SVI at multiparametric MRI and PET/MRI by using a five-point Likert-type scale. The prostatectomy specimen served as the reference standard. Accuracy was assessed with a multireader multicase analysis and by calculating reader-average areas under the receiver operating characteristics curve (AUCs), sensitivity, and specificity for ordinal and dichotomized data in a region-specific and patient-specific approach. Interrater agreement was assessed with the Fleiss multirater κ.

Results: For multiparametric MRI versus PET/MRI in ECE detection, respectively, AUC, sensitivity, and specificity in the region-specific analysis were 0.67 and 0.75 (P = .07), 28% (21 of 76) and 47% (36 of 76) (P = .09), and 94% (529 of 564) and 90% (509 of 564) (P = .007). For the patient-specific analysis, AUC, sensitivity, and specificity were 0.66 and 0.73 (P = .19), 46% (22 of 48) and 69% (33 of 48) (P = .04), and 75% (84 of 112) and 67% (75 of 112) (P = .19), respectively. For multiparametric MRI versus PET/MRI in SVI detection, respectively, AUC, sensitivity, and specificity of the region-specific analysis were 0.66 and 0.74 (P = .21), 35% (seven of 20) and 50% (10 of 20) (P = .25), and 98% (295 of 300) and 94% (282 of 300) ($P < .001$). For the patient-specific analysis, AUC, sensitivity, and specificity were 0.65 and 0.79 (P = .25), 35% (seven of 20) and 55% (11 of 20) (P = .20), and 98% (137 of 140) and 94% (131 of 140) (P = .07), respectively. Interrater reliability for multiparametric MRI versus PET/MRI did not differ for ECE (κ, 0.46 vs 0.40; P = .24) and SVI (κ, 0.23 vs 0.33; P = .39).

Conclusion: Our results suggest that gallium 68 (^{68}Ga)-labeled Glu-urea-Lys (Ahx)-HBED-CC ligand targeting the prostate-specific membrane antigen (PSMA) (^{68}Ga-PSMA-11) PET/MRI and multiparametric MRI perform similarly for local staging of prostate cancer in patients with intermediate-to-high-risk prostate cancer. The increased sensitivity of ^{68}Ga-PSMA-11 PET/MRI for the detection of extracapsular disease comes at the cost of a slightly reduced specificity.

In patients with prostate cancer, the detection of extracapsular extension (ECE) and seminal vesicle invasion (SVI) is not only important for selecting the appropriate therapy but also for preoperative planning of the surgical strategy and for patient prognosis (1,2). The presence of ECE has surgical consequences for pericapsular structures, especially for the neurovascular bundles. Current guidelines recommend performing nerve-sparing radical prostatectomy (RP) in cases of localized disease (3). A high risk of advanced disease, by contrast, is in general a contraindication to nerve-sparing RP (3).

To predict the risk of advanced disease, clinicians often use staging nomograms. While earlier nomograms did not include medical imaging information, recent research has demonstrated an improved accuracy in predicting ECE by incorporating information from multiparametric MRI (4). Multiparametric MRI is a well-established imaging modality in prostate cancer assessment, particularly for depicting clinically significant prostate cancer and improving the yield of transrectal US–guided biopsy (5–8). Moreover, it has been reported to be useful for local staging (9,10) and to have potential to assess prostate cancer aggressiveness (11).

Abbreviations

AUC = area under the ROC curve, CI = confidence interval, ECE = extracapsular extension, MRMC = multireader multicase, PSMA = prostate-specific membrane antigen, ROC = receiver operating characteristic, RP = radical prostatectomy, SVI = seminal vesicle infiltration

Summary

While overall diagnostic performance in local staging of patients with prostate cancer at intermediate to high risk was similar, use of a gallium 68 (^{68}Ga)-labeled Glu-urea-Lys (Ahx)-HBED-CC ligand targeting the prostate-specific membrane antigen (PSMA) (^{68}Ga-PSMA-11) PET/MRI may improve the sensitivity of multiparametric MRI for the detection of extracapsular disease, at the cost of a slightly reduced specificity.

Key Results

- Patient-specific sensitivity for the detection of extracapsular extension of prostate cancer was higher for gallium 68 (^{68}Ga)-labeled Glu-urea-Lys (Ahx)-HBED-CC ligand targeting the prostate-specific membrane antigen (PSMA) (^{68}Ga-PSMA-11) PET/MRI than for multiparametric MRI (69% vs 46%, respectively; $P = .04$.)
- Region-specific specificity for the detection of extracapsular extension and seminal vesicle infiltration was lower for ^{68}Ga-PSMA-11 PET/MRI than for multiparametric MRI (90% vs 94%, $P = .007$ and 94% vs 98%, $P < .001$, respectively).
- There was no difference in the interrater agreement of extracapsular extension and seminal vesicle infiltration estimation between multiparametric MRI and ^{68}Ga-PSMA-11 PET/MRI (Fleiss κ, 0.46 vs 0.40, $P = .24$ and 0.23 vs 0.33, $P = .39$, respectively).

Gallium 68 (^{68}Ga)-labeled Glu-urea-Lys (Ahx)-HBED-CC ligand targeting the prostate-specific membrane antigen (PSMA) (^{68}Ga-PSMA-11) PET is an upcoming imaging modality. It is especially beneficial in the setting of biochemical recurrence of prostate cancer after local treatment. This is mainly because of its superior detection rate compared with conventional imaging and with previously established radiotracers such as radiolabeled choline (12–14).

Recent studies reported additive value of combined ^{68}Ga-PSMA-11 PET and MRI for primary prostate cancer detection (15–17), local recurrence detection after focal therapy (18), and localization (19) compared with multiparametric MRI.

To our knowledge, the potential benefit of ^{68}Ga-PSMA-11 PET/MRI for local staging in patients with intermediate-to-high–risk prostate cancer has not yet been investigated and compared with that of multiparametric MRI. Therefore, the objective of our study was to compare the diagnostic accuracy and interrater agreement of multiparametric MRI and ^{68}Ga-PSMA-11 PET/MRI for the detection of ECE and SVI in patients with prostate cancer.

Materials and Methods

The institutional review board approved this single-center retrospective study, and written informed consent was obtained from all participants.

Patients

We reviewed all consecutive patients undergoing ^{68}Ga-PSMA-11 PET/MRI for primary staging of prostate cancer (n = 103) over a 2-year period (April 2016 through July 2018). Study inclusion criteria were as follows: *(a)* multiparametric MRI within 6 months from PET/MRI and *(b)* subsequent RP at our institution (within 6 months of imaging). Patients were excluded if the multiparametric MRI study was not performed according to current guidelines (20). Risk classification was determined according to the D'Amico classification (21).

Multiparametric MRI Data

MRI was performed with a 1.5-T (10% [four of 40]) or a 3.0-T (90% [36 of 40]) whole-body MRI system at different institutions (n = 29 in house, n = 11 externally performed). The protocol was in accordance with proposed technical requirements of current guidelines (20). At our institution, the typical multiparametric MRI protocol consisted of T2-weighted fast spin-echo images covering the prostate gland and the seminal vesicles, which were obtained in three planes (transverse, sagittal, and coronal). Diffusion-weighted imaging was performed in the transverse plane with identical orientation as the T2-weighted images. The apparent diffusion coefficient parametric maps were calculated by using three b values (0, 50, and 1000 sec/mm^2 or 100, 600, and 1000 sec/mm^2). A high–b-value image (1400 sec/mm^2) was calculated. Dynamic contrast material–enhanced MRI was performed to yield transverse sections with a temporal resolution of less than 8 seconds. Gadoterate meglumine (Dotarem; Guerbet, Darmstadt, Germany) was used as a contrast agent in a dose of 0.1 mmol per kilogram of body weight. The typical MRI protocol included T2-weighted images in three planes, diffusion-weighted imaging, and dynamic contrast-enhanced imaging.

Data Acquisition with ^{68}Ga-PSMA-11 PET/MRI

All PET/MRI data were acquired with a 3.0-T hybrid scanner (SIGNA PET/MR; GE Healthcare, Waukesha, Wis) at our institution. The spatial resolution (full width at half maximum) for ^{68}Ga was 5.46, 5.26, and 6.10 mm (in the x, y, and z directions, respectively) in air and 5.63, 4.77, and 6.47 mm (in the x, y, and z direction, respectively) in water (22). Patients underwent ^{68}Ga-PSMA-11 PET/MRI 60 minutes after a single injection of ^{68}Ga-PSMA-11 (mean dose, 131 MBq ± 18.8 [standard deviation]; range, 98–158 MBq). To reduce tracer activity in the bladder, furosemide (0.13 mg/kg) was injected intravenously 30 minutes prior to the tracer injection, and patients were asked to void prior to scanning. The institutional PET protocol was in agreement with the European Association of Nuclear Medicine and Society of Nuclear Medicine and Molecular Imaging procedure guidelines (23). In brief, the protocol consists of six bed positions with 2–3 minutes acquisition time per bed position for the head to mid-thigh protocol and additional specific sequences covering the pelvis, including a high-resolution T1-weighted LAVA-FLEX sequence (GE Healthcare, Waukesha, Wis), a T2-weighted fast recovery fast spin-echo sequence in at least two planes, and diffusion-weighted imaging. Three-dimensional PET emission data were reconstructed by using time-of-flight information and a fully three-dimensional iterative algorithm, which is part of the manufacturer-supplied standard scanner software (ordered subset expectation maximization–based VUE Point FX; GE Healthcare). The recon-

Table 1: Summary of Characteristics in 40 Patients

Characteristic	Datum
Age (y)*	63 ± 6
PSA level (ng/mL)†	8.12 (7.56)
Gleason score at biopsy	
3 + 4	2 (5)
4 + 3	6 (15)
4 + 4	21 (52.5)
4 + 5	10 (25)
5 + 4	1 (2.5)
Risk according to D'Amico classification	
Intermediate	8 (20)
High	32 (80)
Tumor stage	
pT2a	2 (5)
pT2b	1 (2.5)
pT2c	24 (60)
pT3a	8 (20)
pT3b	5 (12.5)
Time between multiparametric MRI and ^{68}Ga-PSMA-11 PET/MRI (mo)*	3 ± 2
Time between last imaging and operation (mo)*	1 ± 1

Note.—Unless otherwise specified, data are numbers of patients, with percentages in parentheses. ^{68}Ga-PSMA-11 = gallium 68–labeled ^{68}Ga-labeled (Glu-urea-Lys (Ahx)-HBED-CC) ligand targeting the prostate-specific membrane antigen, PSA = prostate-specific antigen.

* Data are means ± standard deviations.

† Data are medians, with interquartile ranges in parentheses.

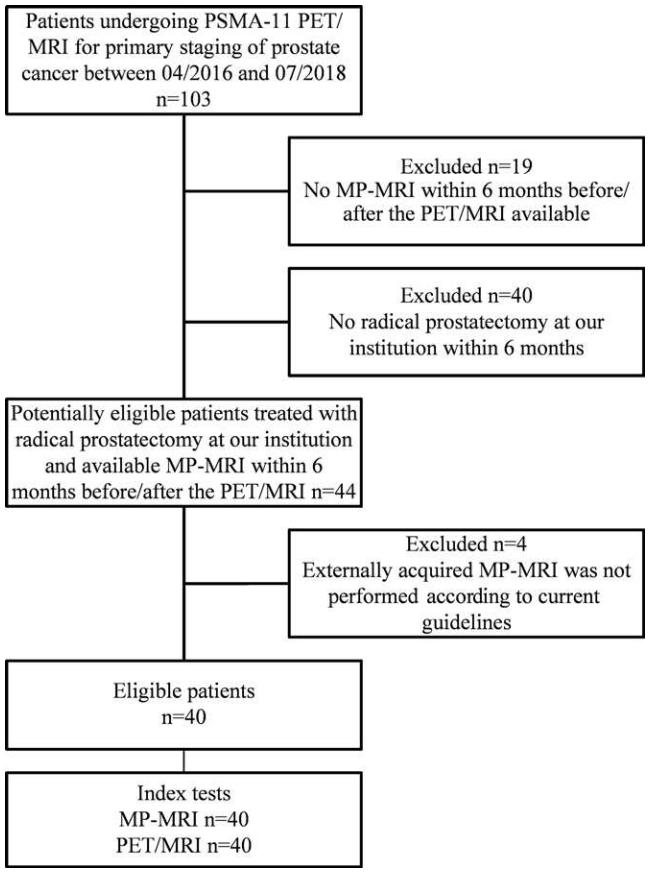

Figure 1: Patient flowchart. MP = multiparametric, PSMA-11 = gallium 68-labeled (Glu-urea-Lys (Ahx)-HBED-CC) ligand targeting the prostate-specific membrane antigen.

struction included standard scatter, dead-time, random attenuation, and normalization correction, as well as correction for the detector response by using Sharper (GE Healthcare). All reconstructions were postfiltered in image space by using an in-plane Gaussian convolution kernel with a full width at half-maximum of 5.0 mm, followed by a standard axial filter with a 3-second kernel using relative weights of 1:4:1. The reconstruction diameter was 60 cm, and the image grid was 256 × 256 with 2.34 × 2.34 × 2.78 mm^3 voxels.

Image Analysis

Four board-certified radiologists (C.S.R. [reviewer 1], A.M.H. [reviewer 2], K.S. [reviewer 3], and A.S.B. [reviewer 4]) with 7 years, 5 years, 1 year, and 1 year of experience in urogenital

Table 2: Reader-Average Diagnostic Accuracy of Multiparametric MRI and ^{68}Ga-PSMA-11 PET/MRI for the Detection of ECE and SVI

Parameter	Multiparametric MRI	^{68}Ga-PSMA-11 PET/MRI	*P* Value
Region-specific ECE			
AUC	0.67 (0.6, 0.73)	0.75 (0.63, 0.87)	.07
Sensitivity (%)	28 (10, 45) [21/76]	47 (23, 71) [36/76]	.09
Specificity (%)	94 (90, 98) [529/564]	90 (86, 94) [509/564]	.007
Patient-specific ECE			
AUC	0.66 (0.65, 0.67)	0.73 (0.72, 0.73)	.19
Sensitivity (%)	46 (42, 50) [22/48]	69 (67, 70) [33/48]	.04
Specificity (%)	75 (74, 76) [84/112]	67 (66, 68) [75/112]	.19
Region-specific SVI			
AUC	0.66 (0.44, 0.88)	0.74 (0.6, 0.88)	.21
Sensitivity (%)	35 (−8, 78) [7/20]	50 (19, 81) [10/20]	.25
Specificity (%)	98 (96, 100) [295/300]	94 (90, 98) [282/300]	<.001
Patient-specific SVI			
AUC	0.65 (0.62, 0.68)	0.79 (0.78, 0.81)	.25
Sensitivity (%)	35 (26, 44) [7/20]	55 (51, 59) [11/20]	.20
Specificity (%)	98 (98, 98) [137/140]	94 (93, 94) [131/140]	.07

Note.—Data in parentheses are 95% confidence intervals; data in brackets are raw data. AUC = area under the receiver operating characteristic curve, ECE = extracapsular extension, ^{68}Ga-PSMA-11 = gallium 68–labeled (Glu-urea-Lys (Ahx)-HBED-CC) ligand targeting the prostate-specific membrane antigen,
SVI = seminal vesicle invasion.

Table 3: Reader-Specific Diagnostic Accuracy of Multiparametric MRI and ^{68}Ga-PSMA-11 PET/MRI for the Detection of ECE and SVI

	ECE		SVI	
Parameter and Reader	Multiparametric MRI	^{68}Ga-PSMA-11 PET/MRI	Multiparametric MRI	^{68}Ga-PSMA-11 PET/MRI
Region specific				
AUC				
Reader 1	0.65 (0.64, 0.65)	0.74 (0.74, 0.75)	0.69 (0.66, 0.72)	0.77 (0.74, 0.8)
Reader 2	0.67 (0.66, 0.68)	0.71 (0.7, 0.72)	0.70 (0.67, 0.72)	0.67 (0.64, 0.7)
Reader 3	0.70 (0.69, 0.7)	0.77 (0.77, 0.78)	0.57 (0.54, 0.6)	0.76 (0.73, 0.79)
Reader 4	0.65 (0.64, 0.66)	0.78 (0.77, 0.79)	0.68 (0.65, 0.71)	0.77 (0.74, 0.8)
Sensitivity (%)				
Reader 1	26 (24, 28) [5/19]	32 (30, 33) [6/19]	40 (28, 52) [2/5]	40 (28, 52) [2/5]
Reader 2	16 (12, 20) [3/19]	37 (34, 39) [7/19]	40 (32, 48) [2/5]	40 (28, 52) [2/5]
Reader 3	32 (30, 34) [6/19]	53 (51, 54) [10/19]	20 (8, 32) [1/5]	60 (48, 72) [3/5]
Reader 4	37 (32, 42) [7/19]	68 (65, 72) [13/19]	40 (28, 52) [2/5]	60 (48, 72) [3/5]
Specificity (%)				
Reader 1	94 (94, 94) [132/141]	92 (92, 92) [130/141]	100 (100, 100) [75/75]	96 (96, 96) [72/75]
Reader 2	97 (97, 97) [137/141]	93 (93, 93) [131/141]	100 (100, 100) [75/75]	96 (96, 96) [72/75]
Reader 3	94 (94, 94) [133/141]	89 (89, 89) [126/141]	97 (97, 97) [73/75]	92 (92, 92) [69/75]
Reader 4	90 (90, 90) [127/141]	87 (86, 87) [122/141]	96 (96, 96) [72/75]	92 (92, 92) [69/75]
Patient specific				
AUC				
Reader 1	0.66 (0.64, 0.68)	0.7 (0.68, 0.71)	0.67 (0.64, 0.71)	0.87 (0.85, 0.89)
Reader 2	0.62 (0.6, 0.64)	0.69 (0.68, 0.71)	0.69 (0.66, 0.72)	0.77 (0.74, 0.8)
Reader 3	0.68 (0.67, 0.7)	0.76 (0.75, 0.78)	0.56 (0.54, 0.59)	0.77 (0.73, 0.8)
Reader 4	0.69 (0.68, 0.71)	0.75 (0.74, 0.76)	0.67 (0.64, 0.7)	0.76 (0.73, 0.79)
Sensitivity (%)				
Reader 1	42 (37, 46) [5/12]	58 (54, 63) [7/12]	40 (28, 52) [2/5]	60 (48, 72) [3/5]
Reader 2	25 (22, 28) [3/12]	58 (54, 63) [7/12]	40 (28, 52) [2/5]	40 (28, 52) [2/5]
Reader 3	42 (37, 46) [5/12]	67 (63, 71) [8/12]	20 (12, 28) [1/5]	60 (48, 72) [3/5]
Reader 4	75 (72, 78) [9/12]	92 (90, 93) [11/12]	40 (28, 52) [2/5]	60 (48, 72) [3/5]
Specificity (%)				
Reader 1	75 (74, 76) [21/28]	75 (74, 76) [21/28]	100 (100, 100) [35/35]	94 (94, 95) [33/35]
Reader 2	86 (85, 87) [24/28]	68 (66, 69) [19/28]	100 (100, 100) [35/35]	97 (97, 97) [34/35]
Reader 3	75 (74, 76) [21/28]	68 (66, 69) [19/28]	97 (97, 97) [34/35]	91 (91, 92) [32/35]
Reader 4	64 (63, 66) [18/28]	57 (55, 59) [16/28]	94 (94, 95) [33/35]	91 (91, 92) [32/35]

Note.—Data in parentheses are 95% confidence intervals; data in brackets are raw data. AUC = area under the receiver operating characteristic curve, ECE = extracapsular extension, ^{68}Ga-PSMA-11 = gallium 68–labeled (Glu-urea-Lys (Ahx)-HBED-CC) ligand targeting the prostate-specific membrane antigen, SVI = seminal vesicle invasion.

radiology and 6 years, 1 year, 1 year, and 1 year of experience in hybrid imaging, respectively, rated the probability of *(a)* ECE in four regions (anterior/posterior part of the prostate on right/left side) and *(b)* SVI in two regions (right/left side) on images from multiparametric MRI and PET/MRI by using a five-point Likert-type scale (where 1 = absent, 2 = probably absent, 3 = equivocal, 4 = probably present, and 5 = definitively present). Estimations of the probability of ECE/SVI were subjective and guided by features of the Prostate Imaging Reporting and Data System, or PI-RADS, version 2 (20) for multiparametric MRI (ie, for ECE invasion or asymmetry of the neurovascular bundles, an irregular or spiculated prostatic margin, a bulging prostatic contour, obliteration of the rectoprostatic angle, a tumor-capsule interface of greater than 1.0 cm, breakthrough of the capsule with evidence of direct tumor extension or bladder wall invasion and SVI, focal or diffuse low T2-weighted signal intensity and/or abnormal contrast material enhancement within and/or along the seminal vesicle, restricted diffusion, obliteration of the angle between the base of the prostate and the seminal vesicle, and demonstration of direct tumor extension from the base of the prostate into or around the seminal vesicle). For PET/MRI, identical features, with the addition of pathologic ^{68}Ga-PSMA-11 accumulation (ie, tracer uptake exceeding that of background tissue) outside of the prostate and within and/or along the seminal vesicle were used.

Anonymized and randomly ordered image studies were reviewed independently in two sessions in this order: *(a)* multiparametric MRI on a standard picture archiving and communication system workstation (AGFA Healthcare, Mortsel, Belgium) and *(b)* PET/MRI on a standard workstation (Advantage Workstation, version 4.6; GE Healthcare). All readers were blinded to clinical and histopathologic findings. An interval of more than

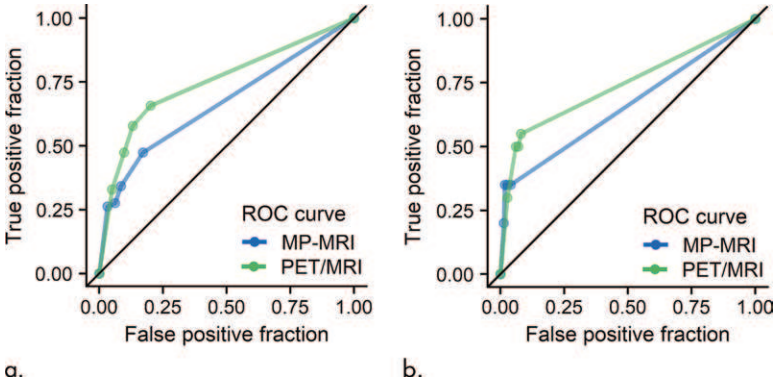

Figure 2: Graphs show the average receiver operating characteristic (ROC) curves of four readers for multiparametric (MP) MRI (blue curve) and gallium 68 (^{68}Ga)-labeled Glu-urea-Lys (Ahx)-HBED-CC ligand targeting the prostate-specific membrane antigen (^{68}Ga-PSMA-11) PET/MRI (green curve) for the region-specific detection of **(a)** extracapsular extension (area under the ROC curve [AUC], 0.67 [95% confidence interval {CI}: 0.6, 0.73] and 0.75 [95% CI: 0.63, 0.8], *P* = .07, respectively) and **(b)** seminal vesicle infiltration (AUC, 0.66 [95% CI: 0.44, 0.88] and 0.74 [95% CI: 0.6, 0.88], *P* = .21, respectively) of prostate cancer.

3 weeks between the reading sessions was maintained to avoid recall bias.

Reference Standard

Pathologic stage at RP was used as the reference standard for ECE and SVI. Histologic findings in all cases were reevaluated by two experienced genitourinary pathologists (N.J.R., J.H.R.) unblinded to clinical information and blinded to all imaging results, using a standard protocol. Mutual agreement for extraprostatic extension was achieved. All regions showing histologic extraprostatic extension (according to the International Society of Urological Pathology consensus conference), including SVI, were documented individually.

Statistical Analysis

All statistical analyses were performed in R (version 3.5.1; R Foundation for Statistical Computing, Vienna, Austria. *https://www.R-project.org/*). Patient demographics and baseline clinical characteristics were summarized by using descriptive statistics. Frequency distribution with percentages was used to summarize categorical variables, and means with standard deviations or medians with interquartile ranges were used to describe continuous variables. Diagnostic accuracy for detection of ECE and SVI was analyzed in four different approaches for each reader and modality. Likert scale points were used for receiver operating characteristics (ROC) analysis and calculation of the area under the ROC curve (AUC) for region-specific detection. The highest Likert scale point per patient was determined for ROC analysis and calculation of the AUC for patient-specific detection. Sensitivity and specificity were calculated on dichotomized data (Likert scale points were dichotomized as ≤ 3 = negative vs > 3 = positive) for region-specific and patient-specific ECE and SVI detection. For the region-specific approach, any region with

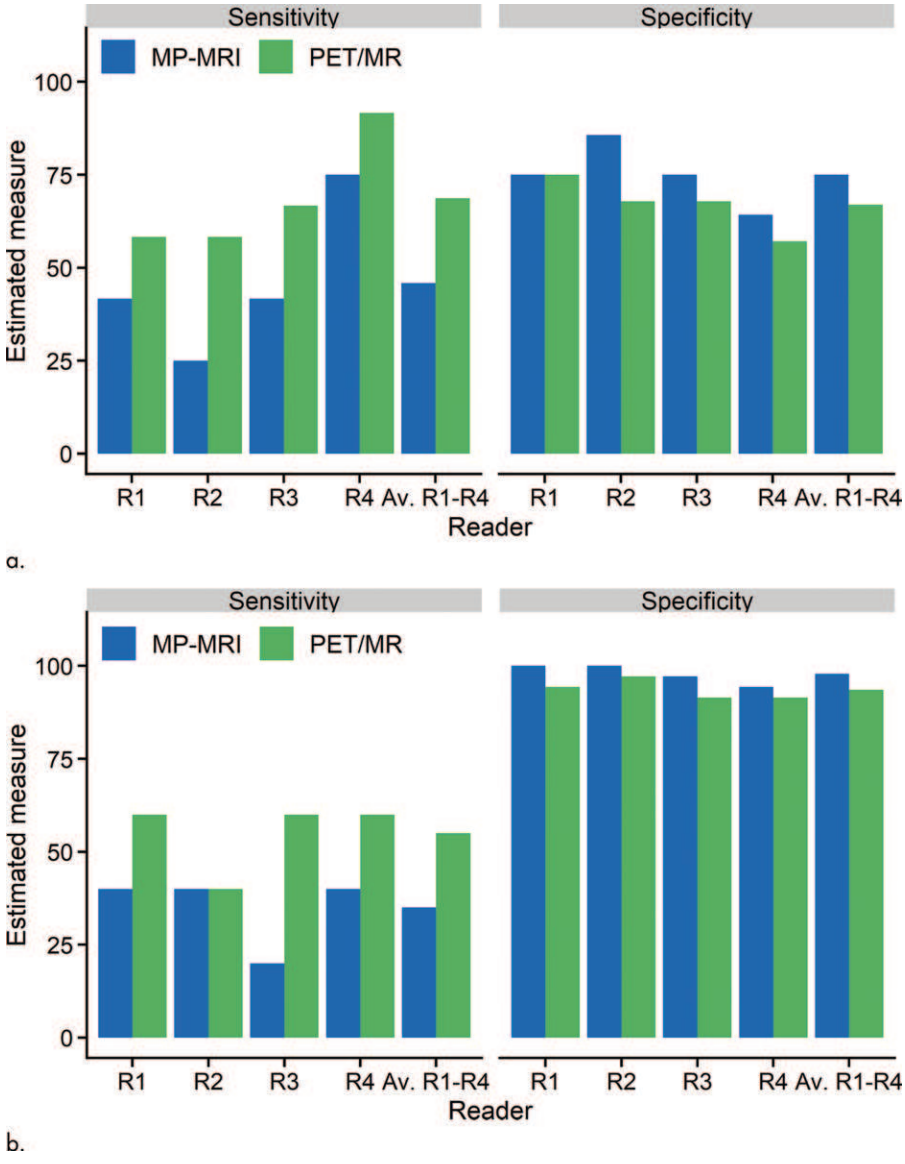

Figure 3: Bar graphs show sensitivity and specificity of multiparametric (MP) MRI (blue) compared with gallium 68 (^{68}Ga)-labeled Glu-urea-Lys (Ahx)-HBED-CC ligand targeting the prostate-specific membrane antigen (^{68}Ga-PSMA-11) PET/MRI (green) for four readers (R1, R2, R3, R4), and reader-average sensitivity and specificity values (Av. R1-R4) for the patient-specific detection of **(a)** extracapsular extension and **(b)** seminal vesicle infiltration.

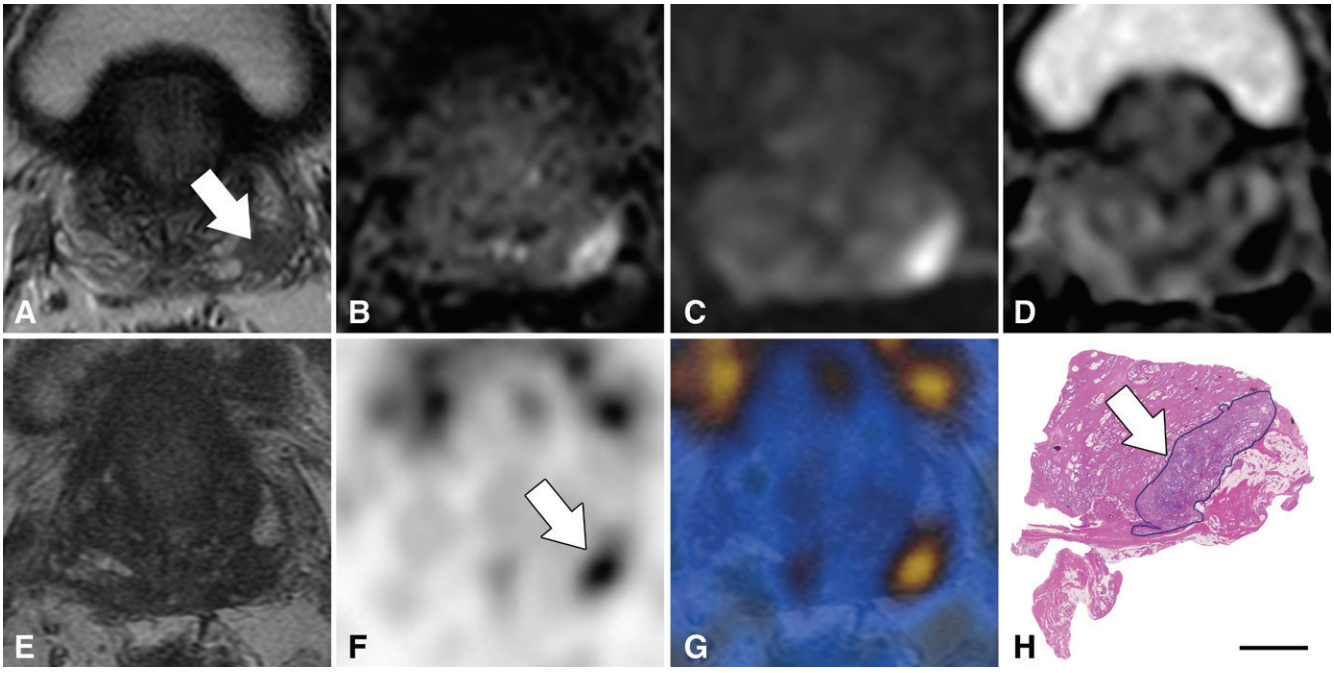

Figure 4: *A–D,* Images from axial multiparametric MRI and, *E–G,* corresponding images from gallium 68 (^{68}Ga)-labeled Glu-urea-Lys (Ahx)-HBED-CC ligand targeting the prostate-specific membrane antigen (^{68}Ga-PSMA-11) PET/MRI in a 65-year-old man with a prostate-specific antigen level of 4.2 ng/mL. *A,* T2-weighted image, *B,* dynamic contrast-enhanced image, *C,* diffusion-weighted image (*b* = 1400 sec/mm^2) and, *D,* corresponding apparent diffusion coefficient map show low T2 signal intensity in the left posterior peripheral zone (arrow) with corresponding restricted diffusion. *E,* T2-weighted image, *F,* PET image (standardized uptake value range, 0–8) and, *G,* fused PET/MRI image show focal radiotracer uptake in the left posterior peripheral zone on the left (arrow). One of four readers rated the images from multiparametric MRI as positive for extraprostatic extension, whereas three of four readers rated the images from PET/MRI positive for extraprostatic extension. *H,* Histopathologic slide of the basal posterior left prostate confirms the presence of tumor with extraprostatic extension (arrow), including extension beyond the prostatic contour and infiltration into fat tissue. (Hematoxylin-eosin stain; scale bar = 5 mm.)

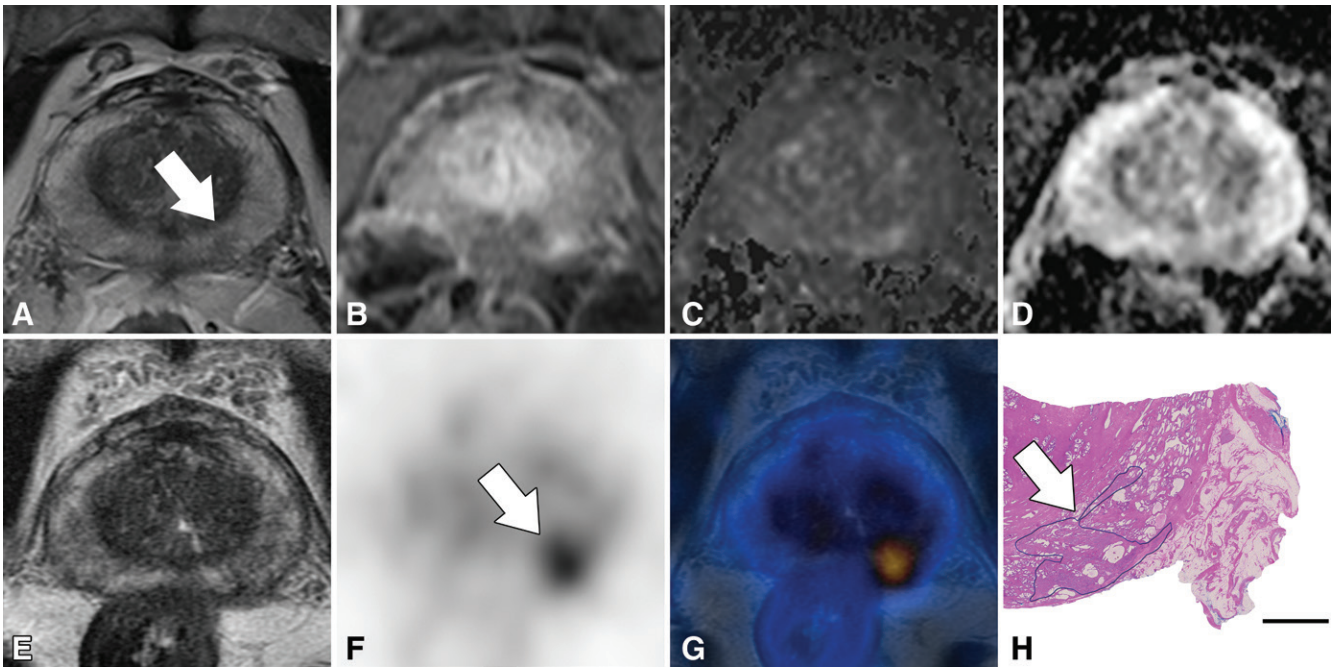

Figure 5: *A–D,* Images from axial multiparametric MRI and, *E–G,* corresponding images from gallium 68 (^{68}Ga)-labeled Glu-urea-Lys (Ahx)-HBED-CC ligand targeting the prostate-specific membrane antigen (^{68}Ga-PSMA-11) PET/MRI in a 72-year-old man with a prostate-specific antigen level of 26.5 ng/mL. *A,* T2-weighted image, *B,* dynamic contrast-enhanced image, *C,* diffusion-weighted image (*b* = 1400 sec/mm^2), and, *D,* corresponding apparent diffusion coefficient map show low T2 signal intensity in the left posterior peripheral zone (arrow) with corresponding restricted diffusion. *E,* T2-weighted image, *F,* PET image (standardized uptake value range, 0–8) and, *G,* fused PET/MRI image show focal radiotracer uptake in the left posterior peripheral zone on the left (arrow). Three of four readers rated the multiparametric MRI as negative for extraprostatic extension, whereas all rated the PET/MRI positive for extraprostatic extension. *H,* Histopathologic slide of midprostate confirms a small focus of prostate carcinoma in the left posterior peripheral zone (arrow) without extraprostatic extension. (Hematoxylin-eosin stain; scale bar = 5 mm.)

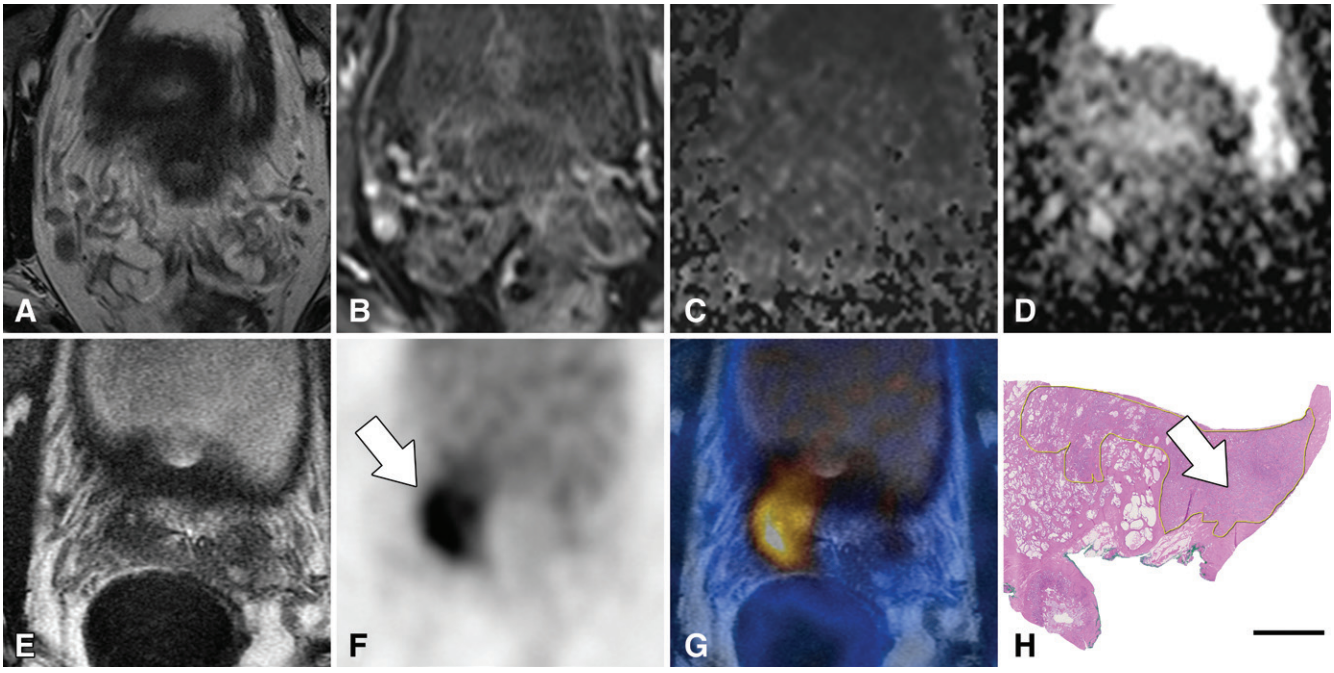

Figure 6: *A–D,* Axial multiparametric MRIs and, *E–G,* corresponding images from gallium 68 (^{68}Ga)-labeled Glu-urea-Lys (Ahx)-HBED-CC ligand targeting the prostate-specific membrane antigen (^{68}Ga-PSMA-11) PET/MRI in a 62-year-old man with a prostate-specific antigen level of 12.83 ng/mL. Full image correlation is limited due to differences in the filling of the urinary bladder. *A,* T2-weighted image, *B,* dynamic contrast-enhanced image, *C,* diffusion-weighted image (*b* = 1400 sec/mm^2), and, *D,* corresponding apparent diffusion coefficient map show unremarkable right seminal vesicle. *E,* T2-weighted image, *F,* PET image (standardized uptake value range, 0–8) and, *G,* fused PET/MRI image show focal ^{68}Ga-PSMA-11 uptake in the right seminal vesicle (arrow). All four readers rated the multiparametric MRI as negative for seminal vesicle invasion, whereas three of four readers rated the PET/MRI positive for seminal vesicle infiltration on the right. *H,* Histopathologic slide of the base of the prostate and right seminal vesicle confirms presence of tumor in the right peripheral zone (arrow) without seminal vesicle infiltration on the right side. (Hematoxylin-eosin stain; scale bar = 5 mm.)

ECE/SVI identified at histopathologic examination that corresponded to the same region with tumor graded as positive at imaging was considered as a true-positive finding, whereas regions negative for tumor at pathologic examination with corresponding regions graded as negative for tumor at imaging were considered as true-negative findings. For the patient-specific approach, all patients with at least one positive region were considered as positive for disease and all patients with no positive regions were considered as negative for disease.

To calculate reader-average AUC, sensitivity, and specificity, as well as to compare these estimates between multiparametric MRI and PET/MRI, a multireader multicase (MRMC) approach including *U* statistics was used (24,25). To account for the correlation of the clustered data (ie, multiple measurement within each patient) the method proposed by Obuchowski was applied (26). Interrater reliability was calculated with the Fleiss multirater κ and compared by using the Hotelling T^2 test (27). Two-sided *P* values of less than .05 were considered to indicate statistically significant differences.

Results

Patient characteristics are summarized in Table 1. Figure 1 shows the patient flowchart. Forty patients were eligible for our study. The mean age of the patients was 63 years (range, 51–78 years). Eighty percent (32 of 40) of the patients had a high-risk setting, and 20% (eight of 40) had an intermediate-risk setting according to the D'Amico classification. Histologic examination revealed 8.5% (19 of 160) of the regions as positive for ECE in 30% (12 of 40) of the patients and 6.3% (five of 80) of the regions as positive for SVI in 12.5% (five of 40) of the patients.

Diagnostic Accuracy for the Detection of ECE

For multiparametric MRI versus PET/MRI, respectively, the region-specific MRMC analysis results were as follows: AUC, 0.67 (95% confidence interval [CI]: 0.6, 0.73) and 0.75 (95% CI: 0.63, 0.87), *P* = .08; sensitivity, 28% (21 of 76) (95% CI: 1%, 45%) and 47% (36 of 76) (95% CI: 23%, 71%), *P* = .09; and specificity, 94% (529 of 564) (95% CI: 90%, 98%) and 90% (509 of 564) (95% CI: 86%, 94%), *P* = .007. Reader-specific AUC ranged from 0.65 to 0.70 for multiparametric MRI and from 0.71 to 0.78 for PET/MRI. Table 2 summarizes reader-average accuracy results, and Table 3 summarizes reader-specific accuracy results. Reader-average ROC curves of the region-specific analysis of the readers are illustrated in Figure 2, indicating higher AUCs for PET/MRI.

For multiparametric MRI versus PET/MRI, respectively, the patient-specific MRMC analysis results were as follows: AUC, 0.66 (95% CI: 0.65, 0.67) and 0.73 (95% CI: 0.72, 0.73), *P* = .19; sensitivity, 46% (22 of 48) (95% CI: 42%, 50%) and 69% (33 of 48) (95% CI: 67%, 70%), *P* = .04; and specificity, 75% (84 of 112) (95% CI: 74%, 76%) and 67% (75 of 112) (95% CI: 66%, 68%), *P* = .19. Figure 3a illustrates the differences in sensitivities and specificities between multiparametric MRI and PET/MRI for the patient-specific

approach and shows that all four readers achieved higher sensitivity with PET/MRI. Figures 4 and 5 show examples of discordant multiparametric MRI and PET/MRI findings; while Figure 4 depicts a case with a majority of false-negative ECE multiparametric MRI image interpretations (three of four readers), Figure 5 shows a case with false-positive ECE PET/MRI image interpretations for all readers.

Diagnostic Accuracy for the Detection of SVI

For multiparametric MRI versus PET/MRI, respectively, the region-specific MRMC analysis results were as follows: AUC, 0.66 (95% CI: 0.44, 0.88) and 0.74 (95% CI: 0.6, 0.88), P = .21; sensitivity, 35% (seven of 20) (95% CI: –8%, 78%) and 50% (10 of 20) (95% CI: 19%, 81%), P = .25; and specificity, 98% (295 of 300) (95% CI: 96%, 100%) and 94% (282 of 300) (95% CI: 90%, 98%), $P < .001$. Reader-specific AUC ranged from 0.57 to 0.70 for multiparametric MRI and from 0.67 to 0.77 for PET/MRI. Figure 3b illustrates the differences in sensitivities and specificities between multiparametric MRI and PET/MRI for the patient-specific approach and shows that all readers achieved a slightly lower specificity in the detection of SVI with PET/MRI. Table 2 summarizes reader-average accuracy results, and Table 3 summarizes reader-specific accuracy results.

For multiparametric MRI versus PET/MRI, respectively, the patient-specific MRMC analysis results were as follows: AUC, 0.65 (95% CI: 0.62, 0.68) and 0.79 (95% CI: 0.78, 0.81), P = .25; sensitivity, 35% (seven of 20) (95% CI: 26%, 44%) and 55% (11 of 20) (95% CI: 51%, 59%), P = .20; and specificity, 98% (137 of 140) (95% CI: 98%, 98%) and 95% (131 of 140) (95% CI: 93%, 94%), P = .07. Figure 6 shows an example of discordant multiparametric MRI and PET/MRI findings with a majority of false-positive SVI PET/MRI image interpretations (three of four readers).

Interrater Reliability

The Fleiss κ for the rating of the probability of ECE was 0.46 (95% CI: 0.36, 0.55) for multiparametric MRI and 0.40 (95% CI: 0.33, 0.47) for PET/MRI, P = .24. The Fleiss κ for the rating of the probability of SVI was 0.23 (95% CI: 0.10, 0.46) for multiparametric MRI and 0.33 (95% CI: 0.17, 0.25) for PET/MRI, P = .39.

Discussion

The potential benefit of gallium 68 (^{68}Ga)-labeled Glu-urea-Lys (Ahx)-HBED-CC ligand targeting the prostate-specific membrane antigen (PSMA) (^{68}Ga-PSMA-11) PET/MRI for local staging in patients with intermediate-to-high–risk prostate cancer has not yet been investigated and compared with multiparametric MRI. In our study, including 40 patients with intermediate-to-high–risk prostate cancer undergoing multiparametric MRI and ^{68}Ga-PSMA-11 PET/MRI before RP, we found that ^{68}Ga-PSMA-11 PET/MRI increased the sensitivity for the detection of ECE of prostate cancer (69% [33 of 48] vs 46% [22 of 48], respectively; P = .04) with a slight reduction in specificity (90% [509 of 564] vs 94% [529 of 564], respectively; P = .007) compared with multiparametric MRI. Moreover, we found a slight reduction in specificity (94% [282 of 300] vs 98% [295 of 300], respectively; $P < .001$) for the detection of SVI with ^{68}Ga-PSMA-11 PET/MRI compared with multiparametric MRI. However, in the region-specific analysis, we did not find a difference in sensitivity for the detection of ECE and SVI with ^{68}Ga-PSMA-11 PET/MRI. On the other hand, specificity in detection of ECE and SVI was higher with multiparametric MRI than with ^{68}Ga-PSMA-11 PET/MRI.

Combining the functional information from ^{68}Ga-PSMA-11 PET with the well-established technique of multiparametric MRI might explain the higher sensitivity for the detection of locally advanced disease. Previous studies reported improved sensitivity for primary prostate cancer detection for ^{68}Ga-PSMA-11 PET/MRI compared with multiparametric MRI (15,16), which might allow the reader to focus on locally advanced disease in the regions suspected of harboring primary prostate cancer. One reason the rather small differences in specificity of region-specific ECE and SVI were statistically significant and the rather large differences in sensitivity were not may be because specificity was based on many (eg, for ECE, n = 141) true-negative events and sensitivity was based on rather few true-positive events (eg, for ECE, n = 19), which is an inherent limitation of the sample distribution in our cohort. Several factors leading to false-positive findings could explain the slightly lower specificity of ^{68}Ga-PSMA-11 PET/MRI (28). Moreover, high accumulation of ^{68}Ga-PSMA-11 in aggressive tumors can lead to spillover of activity into normal tissue, as has previously been described in choline PET/CT for local staging of prostate cancer (29). Spatial resolution of T2-weighted images is essential for adequate local staging (20). Therefore, differences in signal-to-noise ratio or spatial resolution of the images from PET/MRI and MRI may also play an important role in the evaluation of locally advanced disease in patients with prostate cancer.

Current studies investigating the diagnostic accuracy of multiparametric MRI for the detection of ECE using a comparable imaging protocol showed similar accuracy compared with our study results. Mehralivand et al (30) reported an AUC of 0.77 for the detection of extraprostatic extension in a cohort of 553 patients using a newly introduced grading system for extraprostatic extension. Krishna et al (31) reported a sensitivity of 43% and a specificity of 91.3% and an AUC of 0.67 for the detection of ECE in a cohort of 149 patients. The higher sensitivity of 66% for the detection of SVI reported by Soylu et al (32) may in part be explained by the use of an endorectal coil in their cohort, which was paralleled by a substantial increase in signal-to-noise ratio (21).

Only a few studies have investigated the diagnostic accuracy of PSMA PET for the detection of ECE and SVI. Thalgott et al (33) reported comparable AUCs of 0.70 for ECE and 0.81 for SVI using ^{68}Ga PSMA-11 PET/MRI in a cohort of 73 patients. Fendler et al (34) reported similar values of sensitivity and specificity for ECE and SVI detection. von Klot et al (35) reported a higher sensitivity of 90% and a similar specificity of 91% for the detection of ECE and similar values (75% and 100%) for the detection of SVI using ^{68}Ga PSMA-I&T PET/CT in a small cohort of 21 patients.

The main limitations of our study were the small sample size, which was partially mitigated by MRMC analysis, and its retrospective nature, which entails a selection bias. Our results apply to a selected group of patients with intermediate-to-high–risk prostate cancer who are therefore more likely to overexpress PSMA and have a higher T-stage at presentation. The results from our study may therefore not apply to populations including patients with low-risk prostate cancer. However, ^{68}Ga-PSMA-11 PET/MRI is usually performed in patients with higher-risk prostate cancer for exclusion of distant disease. Because of time constraints during the PET/MRI examination, our PET/MRI protocol did not include a dynamic contrast-enhanced sequence, which might have limited the accuracy of SVI detection. In addition, the parameters for multiparametric MRI were not homogeneous (n = 11 multiparametric MRI studies were acquired at external institutions).

In conclusion, our results suggest that gallium 68 (^{68}Ga)-labeled Glu-urea-Lys (Ahx)-HBED-CC ligand targeting the prostate-specific membrane antigen (PSMA) (^{68}Ga-PSMA-11) PET/MRI and multiparametric MRI perform similarly in local staging of prostate cancer in patients with intermediate-to-high–risk prostate cancer. The increased sensitivity of ^{68}Ga-PSMA-11 PET/MRI for the detection of extracapsular disease comes at the cost of a slightly reduced specificity.

Acknowledgments: The authors thank Brandon D. Gallas, PhD, for his statistical advice, as well as the Sick legat and the Iten-Kohaut foundations for their financial support.

Author contributions: Guarantors of integrity of entire study, I.A.B., O.F.D.; study concepts/study design or data acquisition or data analysis/interpretation, all authors; manuscript drafting or manuscript revision for important intellectual content, all authors; approval of final version of submitted manuscript, all authors; agrees to ensure any questions related to the work are appropriately resolved, all authors; literature research, U.J.M., I.A.B., A.S.B., K.S., N.J.R., J.H.R., O.F.D.; clinical studies, U.J.M., I.A.B., K.S., A.M.H., C.S.R., J.M., O.F.D.; experimental studies, J.H.R.; statistical analysis, U.J.M., A.S.B.; and manuscript editing, all authors

Disclosures of Conflicts of Interest: **U.J.M.** disclosed no relevant relationships. **I.A.B.** disclosed no relevant relationships. **A.S.B.** disclosed no relevant relationships. **K.S.** disclosed no relevant relationships. **A.M.H.** disclosed no relevant relationships. **C.S.R.** disclosed no relevant relationships. **J.M.** disclosed no relevant relationships. **N.J.R.** disclosed no relevant relationships. **J.H.R.** disclosed no relevant relationships. **D.E.** disclosed no relevant relationships. **O.F.D.** Activities related to the present article: disclosed no relevant relationships. Activities not related to the present article: is a member of the board of BCRP Holding (containing nonmedicine companies like railway technology and transportation companies); institution has received a grant for clinical USPIO imaging; has been paid for some lectures on MRI. Other relationships: disclosed no relevant relationships.

References

1. Mikel Hubanks J, Boorjian SA, Frank I, et al. The presence of extracapsular extension is associated with an increased risk of death from prostate cancer after radical prostatectomy for patients with seminal vesicle invasion and negative lymph nodes. Urol Oncol 2014;32(1):26.e1–26.e7.
2. Partin AW, Borland RN, Epstein JI, Brendler CB. Influence of wide excision of the neurovascular bundle(s) on prognosis in men with clinically localized prostate cancer with established capsular penetration. J Urol 1993;150(1):142–146; discussion 146–148.
3. Mottet N, Bellmunt J, Bolla M, et al. EAU-ESTRO-SIOG Guidelines on Prostate Cancer. Part 1: Screening, Diagnosis, and Local Treatment with Curative Intent. Eur Urol 2017;71(4):618–629.
4. Martini A, Gupta A, Lewis SC, et al. Development and internal validation of a side-specific, multiparametric magnetic resonance imaging-based nomogram for the prediction of extracapsular extension of prostate cancer. BJU Int 2018;122(6):1025–1033.
5. Johnson LM, Turkbey B, Figg WD, Choyke PL. Multiparametric MRI in prostate cancer management. Nat Rev Clin Oncol 2014;11(6):346–353.
6. Ahmed HU, Arya M, Freeman A, Emberton M. Do low-grade and low-volume prostate cancers bear the hallmarks of malignancy? Lancet Oncol 2012;13(11):e509–e517.
7. Kasivisvanathan V, Rannikko AS, Borghi M, et al. MRI-Targeted or Standard Biopsy for Prostate-Cancer Diagnosis. N Engl J Med 2018;378(19):1767–1777.
8. Verma S, Choyke PL, Eberhardt SC, et al. The Current State of MR Imaging-targeted Biopsy Techniques for Detection of Prostate Cancer. Radiology 2017;285(2):343–356.
9. de Rooij M, Hamoen EHJ, Witjes JA, Barentsz JO, Rovers MM. Accuracy of Magnetic Resonance Imaging for Local Staging of Prostate Cancer: A Diagnostic Meta-analysis. Eur Urol 2016;70(2):233–245.
10. Hoeks CM, Barentsz JO, Hambrock T, et al. Prostate cancer: multiparametric MR imaging for detection, localization, and staging. Radiology 2011;261(1):46–66.
11. Donati OF, Mazaheri Y, Afaq A, et al. Prostate cancer aggressiveness: assessment with whole-lesion histogram analysis of the apparent diffusion coefficient. Radiology 2014;271(1):143–152.
12. Afshar-Oromieh A, Zechmann CM, Malcher A, et al. Comparison of PET imaging with a (68)Ga-labelled PSMA ligand and (18)F-choline-based PET/CT for the diagnosis of recurrent prostate cancer. Eur J Nucl Med Mol Imaging 2014;41(1):11–20.
13. Eissa A, Elsherbiny A, Coelho RF, et al. The role of 68Ga-PSMA PET/CT scan in biochemical recurrence after primary treatment for prostate cancer: a systematic review of the literature. Minerva Urol Nefrol 2018;70(5):462–478.
14. Schwenck J, Rempp H, Reischl G, et al. Comparison of ^{68}Ga-labelled PSMA-11 and ^{11}C-choline in the detection of prostate cancer metastases by PET/CT. Eur J Nucl Med Mol Imaging 2017;44(1):92–101.
15. Hicks RM, Simko JP, Westphalen AC, et al. Diagnostic Accuracy of ^{68}Ga-PSMA-11 PET/MRI Compared with Multiparametric MRI in the Detection of Prostate Cancer. Radiology 2018;289(3):730–737.
16. Park SY, Zacharias C, Harrison C, et al. Gallium 68 PSMA-11 PET/MR Imaging in Patients with Intermediate- or High-Risk Prostate Cancer. Radiology 2018;288(2):495–505.
17. Rhee H, Thomas P, Shepherd B, et al. Prostate Specific Membrane Antigen Positron Emission Tomography May Improve the Diagnostic Accuracy of Multiparametric Magnetic Resonance Imaging in Localized Prostate Cancer. J Urol 2016;196(4):1261–1267.
18. Burger IA, Müller J, Donati OF, et al. 68Ga-PSMA-11 PET/MR Detects Local Recurrence Occult on mpMRI in Prostate Cancer Patients After HIFU. J Nucl Med 2019;60(8):1118–1123.
19. Eiber M, Weirich G, Holzapfel K, et al. Simultaneous ^{68}Ga-PSMA HBED-CC PET/MRI Improves the Localization of Primary Prostate Cancer. Eur Urol 2016;70(5):829–836.
20. Weinreb JC, Barentsz JO, Choyke PL, et al. PI-RADS Prostate Imaging - Reporting and Data System: 2015, Version 2. Eur Urol 2016;69(1):16–40.
21. D'Amico AV, Whittington R, Malkowicz SB, et al. Biochemical outcome after radical prostatectomy, external beam radiation therapy, or interstitial radiation therapy for clinically localized prostate cancer. JAMA 1998;280(11):969–974.
22. Huang SC, Savic D, Yang J, Shrestha U, Seo Y. The effect of magnetic field on positron range and spatial resolution in an integrated whole-body time-of-flight PET/MRI system. 2014 IEEE Nuclear Science Symposium and Medical Imaging Conference (NSS/MIC). Seattle, Wash: IEEE; 2014; 1–4.
23. Fendler WP, Eiber M, Beheshti M, et al. ^{68}Ga-PSMA PET/CT: Joint EANM and SNMMI procedure guideline for prostate cancer imaging: version 1.0. Eur J Nucl Med Mol Imaging 2017;44(6):1014–1024.
24. Gallas BD, Pennello GA, Myers KJ. Multireader multicase variance analysis for binary data. J Opt Soc Am A Opt Image Sci Vis 2007;24(12):B70–B80.
25. Gallas BD, Bandos A, Samuelson FW, Wagner RF. A Framework for Random-Effects ROC Analysis: Biases with the Bootstrap and Other Variance Estimators. Commun Stat Theory Methods 2009;38(15):2586–2603.
26. Obuchowski NA. Nonparametric analysis of clustered ROC curve data. Biometrics 1997;53(2):567–578.
27. Vanbelle S. Comparing dependent kappa coefficients obtained on multilevel data. Biom J 2017;59(5):1016–1034.
28. Hofman MS, Hicks RJ, Maurer T, Eiber M. Prostate-specific Membrane Antigen PET: Clinical Utility in Prostate Cancer, Normal Patterns, Pearls, and Pitfalls. RadioGraphics 2018;38(1):200–217.
29. Giovacchini G, Picchio M, Coradeschi E, et al. Predictive factors of [(11)C]choline PET/CT in patients with biochemical failure after radical prostatectomy. Eur J Nucl Med Mol Imaging 2010;37(2):301–309.
30. Mehralivand S, Shih JH, Harmon S, et al. A Grading System for the Assessment of Risk of Extraprostatic Extension of Prostate Cancer at Multiparametric MRI. Radiology 2019;290(3):709–719.
31. Krishna S, Lim CS, McInnes MDF, et al. Evaluation of MRI for diagnosis of extraprostatic extension in prostate cancer. J Magn Reson Imaging 2018;47(1):176–185.
32. Soylu FN, Peng Y, Jiang Y, et al. Seminal vesicle invasion in prostate cancer: evaluation by using multiparametric endorectal MR imaging. Radiology 2013;267(3):797–806.
33. Thalgott M, Düwel C, Rauscher I, et al. One-Stop-Shop Whole-Body ^{68}Ga-PSMA-11 PET/MRI Compared with Clinical Nomograms for Preoperative T and N Staging of High-Risk Prostate Cancer. J Nucl Med 2018;59(12):1850–1856.
34. Fendler WP, Schmidt DF, Wenter V, et al. 68Ga-PSMA PET/CT Detects the Location and Extent of Primary Prostate Cancer. J Nucl Med 2016;57(11):1720–1725.
35. von Klot CJ, Merseburger AS, Böker A, et al. ^{68}Ga-PSMA PET/CT Imaging Predicting Intraprostatic Tumor Extent, Extracapsular Extension and Seminal Vesicle Invasion Prior to Radical Prostatectomy in Patients with Prostate Cancer. Nucl Med Mol Imaging 2017;51(4):314–322.